Chem. Soc., **93**, 6691 (1971).
10. W. Giggenbach, *Inorg. Chem.*, **10**, 1308 (1971).
11. J. P. Bernard, A. DeHaan, and H. Van der Poorten, *C. R. Acad. Sci. Paris*, **276**, 587 (1973).
12. J. H. Kennedy and F. Adamo, *This Journal*, **119**, 1518 (1972).
13. B. Cleaver, A. J. Davies, and D. J. Schiffrin, *Electrochim. Acta*, **18**, 747 (1973).
14. J. R. Birk and R. K. Steunenberg, *Adv. Chem. Ser.*, **740**, 786 (1975).
15. D. O. Raleigh, J. T. White, and C. A. Ogden, *This Journal*, **126**, 1087 (1979).
16. K. W. Kam and K. E. Johnson, *J. Electroanal. Chem. Interfacial Electrochem.*, **115**, 53 (1980).
17. G. Santarini, *C. R. Acad. Sci. Paris*, **288**, 457 (1979).
18. C. H. Liu, A. J. Zielen, and D. M. Gruen, *This Journal*, **120**, 67 (1973).
19. M. J. Weaver and D. Inman, *Electrochim. Acta*, **20**, 929 (1975).
20. R. S. Nicholson and I. Shain, *Anal. Chem.*, **36**, 706 (1964).
21. D. S. Polcyn and I. Shain, *ibid.*, **38**, 370 (1966).
22. C. P. Andrieux, L. Nadjo, and J. M. Saveant, *J. Electroanal. Chem. Interfacial Electrochem.*, **26**, 147 (1970).
23. G. Mamantov, D. L. Manning, and J. M. Dale, *ibid.*, **9**, 253 (1965).
24. R. C. Vogel *et al.*, Argonne National Laboratory ANL-7775, 120 (1971).
25. M. S. Shuman, *Anal. Chem.*, **41**, 142 (1969).
26. M. L. Saboungi, J. J. Marr, and M. Blander, *This Journal*, **125**, 1567 (1978).
27. M. L. Saboungi, J. J. Marr, and M. Blander, *Metall. Trans.*, **10B**, 477 (1979).
28. T. Berzins and P. Delahay, *J. Am. Chem. Soc.*, **75**, 555 (1953).

Oxygen Transfer on Substituted ZrO_2, Bi_2O_3, and CeO_2 Electrolytes with Platinum Electrodes

I. Electrode Resistance by D-C Polarization

M. J. Verkerk,[1] M. W. J. Hammink, and A. J. Burggraaf

Twente University of Technology, Department of Chemical Engineering, Laboratory of Inorganic Chemistry and Materials Science, 7500 AE Enschede, The Netherlands

ABSTRACT

The electrode behavior of Pt-sputtered and PT-gauze electrodes on ZrO_2-Y_2O_3, Bi_2O_3-Er_2O_3, and CeO_2-Gd_2O_3 solid electrolytes was investigated by means of d-c measurements in the temperature region of 770-1050 K and in the oxygen partial pressure region of 10^{-5} – 1 atm O_2 using N_2-O_2 mixtures. On these different materials the same electrode morphology was realized and was preserved during the subsequent experiments. The electrode process is strongly influenced by the nature of the electrolyte. The electrode resistance for Pt electrodes on Bi_2O_3-Er_2O_3 was found to be many times lower than on ZrO_2-Y_2O_3 and CeO_2-Gd_2O_3. On zirconia- and ceria-based materials diffusion of atomic oxygen on the Pt electrode is the rate-determining step in the electrode process, whereas for bismuth sesquioxide-based materials diffusion on the oxide surfaces is rate determining.

There is a considerable interest in solid electrolytes for use in oxygen sensors, oxygen pumps, and high temperature fuel cells. In these applications the electrode polarization and the electrolyte resistance both play an important role. These effects influence the response of an oxygen sensor and give rise to energy losses and therefore to a decreased efficiency of oxygen pumps and fuel cells. Many studies are performed on electrode processes. However, the dominant elementary steps of the overall process are still unknown in most cases.

The kinetics of the electrode process is strongly influenced by the electrode structure (1-6), electrode material (4, 5, 7-9), and the electrolyte (4, 5, 7). Information about the role of the electrolyte in the electrode process is very scarce and is limited to the role of the dopant. Schouler (4) found that the oxygen partial pressure dependence of the electrode resistance of a sputtered platinum electrode depends on the Y_2O_3 content of the ThO_2 electrolyte. Fabry and Kleitz (7) found that the activation energy of the electrode resistance of a point electrode on calcia-stabilized zirconia is higher than that on yttria-stabilized zirconia. Wang and Nowick (5) reported that the exchange current of a Pt-paste electrode is not influenced by the nature and the concentration of the dopant of the CeO_2 electrolyte.

Even less attention is paid to the influence of the nature of the electrolyte on the overall electrode process. From model considerations this influence has to be expected if particular elementary steps are dominant. In most studies reported in the literature the measurements are performed under different circumstances and using different and badly characterized electrode structures and consequently the results can hardly be compared.

Therefore, we studied the influence of the electrolyte conductivity and electrolyte composition on the electrode kinetics using different oxygen ion conductors. An important condition is that on these different materials the same electrode morphology has to be realized. Sputtered and gauze electrodes, subjected to several treatments, can meet this condition. The comparison of a sputtered and a gauze electrode on the same electrolyte may be a tool for investigating the rate-determining step.

The following systems were investigated:

$(ZrO_2)_{0.83}(YO_{1.5})_{0.17}$ (ZY17)

$(CeO_2)_{0.90}(GdO_{1.5})_{0.10}$ (CG10)

$(Bi_2O_3)_{0.80}(Er_2O_3)_{0.20}$ (BE20)

$(Bi_2O_3)_{0.70}(Er_2O_3)_{0.30}$ (BE30)

$(Bi_2O_3)_{0.60}(Er_2O_3)_{0.40}$ (BE40)

The bulk conductivity of the stabilized bismuth sesquioxides is 10-100 times higher than that of the stabilized zirconias and the substituted cerias (10, 11). Besides, bismuth oxide compounds are used as oxidation catalysts and a relative rapid transfer of oxygen on the solid-gas interface is suggested. For these reasons, we

[1] Present address: Philips Research Laboratories, Eindhoven, The Netherlands.

Key words: electrode resistance, solid electrolytes, Pt electrodes, electrode morphology.

Downloaded 22 Jun 2009 to 130.89.112.86. Redistribution subject to ECS license or copyright; see http://www.ecsdl.org/terms_use.jsp

investigated the idea whether the electrode resistance on the bismuth-based materials might be lower than that on the zirconia- and ceria-based materials.

Special attention is paid to the possibility of using the above-mentioned materials as a solid electrolyte in an oxygen pump. Therefore, the measurements were performed at relatively low temperatures and high oxygen partial pressures.

In this paper a phenomenological description of the influence of the nature of the electrolyte on the electrode process is given (d-c study). In part II of this study (12) the observed influence of the electrolyte is analyzed with respect to its critical steps by means of a frequency dispersion study.

Experimental

Sample preparation and characterization are given in Table I. The composition of the samples was checked with x-ray fluorescence. The diameter of the samples was 5-10 mm and the thickness 0.7-1.5 mm.

Measurements were performed in the temperature range 770-1050 K and with N_2-O_2 mixtures in the oxygen partial pressure range of 10^{-5}-1 atm O_2. The oxygen partial pressures in the range of 10^{-2}-1 atm were obtained by mixing appropriate O_2/N_2 mixtures and in the range of 10^{-5}-10^{-2} atm by an oxygen pump (15, 16). The oxygen partial pressure is measured using an oxygen sensor based on stabilized zirconia. The gases were supplied at a rate of 600 cm³/min.

The electrical circuit used in the d-c experiments is shown in Fig. 1. A Wenking potentiostat was used. The current was measured by the voltage drop across the reference resistor. The voltages were measured with an HP 3465A multimeter. The electrode resistance R_{el} was measured using a voltage of 1-10 mV across the sample and calculated according to

$$R_{el} = \left(\frac{dV}{dI}\right)_{I\to 0} - R_b \qquad [1]$$

The total bulk resistance R_b was obtained from a-c impedance measurements (13).

The complex impedance measurements were performed in the frequency range 10^6-10^{-3} Hz using a Solartron 1174 Frequency Response Analyzer with a sample voltage of 10 mV. The circuit is described in Ref. (13).

Electrode Preparation and Characterization

Platinum electrodes with a thickness of 0.75 μm were sputtered onto the polished samples. The sintering of the electrode during thermal treatments is influenced by the nature of the electrolyte. To obtain the same electrode morphology on different electrolytes a sintering temperature in the region of 1200-1400 K was necessary (2-4 hr). To be sure that no visible changes in the electrode morphology take place during the measurements, the system was equilibrated for 48 hr at the highest measuring temperature, and an a-c current treatment (1 kHz, 1V, 5 min) was applied. A typical scanning electron microscope (SEM, JEOL JSMU 3) picture is given in Fig. 2a. The morphology of the electrode is characterized by the length of the three-phase line and the surface area of the interfaces: electrolyte/electrode, electrolyte/gas, and electrode/gas. These data are given in Table II. The maximum measuring temperature is restricted by the requirement that the morphology of the electrode does not change in time. This condition is satisfied if the maximum measuring temperature is kept 150-200 K below the sintering temperature of the metal electrode. At every temperature the electrode was equilibrated for 16 hr before a measurement was performed.

Table I. Preparation and characterization of the samples

System	Preparation method	Sintering temperature (K)	Density (%)	Grain size (μm)
ZY17	Alkoxide synthesis (13)	1673	99	2.5
CG10	Citrate synthesis (14)	1773	96	5
BE20	Solid-state reaction (10)	1198	95	30
BE30	Solid-state reaction (10)	1273	96	30
BE40	Solid-state reaction (10)	1323	95	30

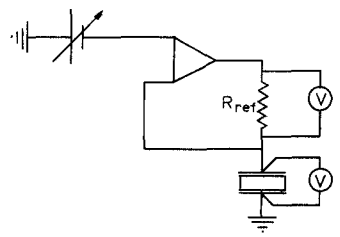

Fig. 1. Electrical circuit for the d-c measurements

Platinum gauze electrodes (200 meshes/cm²) were plastically deformed before use to obtain a reproducible contact surface. An overall picture of the gauze electrode is shown in Fig. 2b and its characteristic data are given in Table II. Figure 2c shows a representative part of the contact surface of a gauze electrode used on ZY17 or CG10 and Fig. 2d shows the same for BE20, BE30, and BE40. From these figures it is clear that because of the roughness of the contact surface oxygen molecules can penetrate this interface. Therefore, the actual three-phase line will be much larger than calculated on the basis of the circumference of the oval flattened parts of the gauze electrode. The gauze electrode was held with a constant pressure on the sample. Before the measurements were performed the above-described thermal and current treatments were applied.

After performing the d-c measurements (1-10 mV) and subsequently the a-c measurements [reported in part II of this study (12)], the electrode resistance was again measured by d.c. (1-10 mV). The total measuring time was about 600 hr. The electrode resistance of the Pt-sputtered electrode on BE20 was increased by a factor of two. Some Er_2O_3 particles could be detected on the electrode surface by means of SEM and x-ray diffraction. The R_{el} for the other combinations was not significantly changed during the measuring period. SEM pictures showed no changes in the morphology of the electrodes. Afterward the same samples were used for d-c experiments in the region of 0-2V.

Reproducibility of the electrode resistance of sputtered and gauze electrodes was checked on three nominally equal electrodes applied on ZY17. The electrode resistance falls in the region of log $R_{el} \pm$ log 1.2 and log $R_{el} \pm$ log 2 for sputtered and gauze electrodes, respectively.

Preliminary experiments on ZY17 with grain sizes of 0.5, 2.5, and 20 μm showed that the electrode resistance is not influenced by the grain size of the electrolyte.

Theory

In this section the relevant theory for the interpretation of the experimental data is given.

Table II. Characteristic data of the morphology of the sputtered (sp) and the gauze (g) electrode

Electrode	Three-phase line length (m/m²)	Electrolyte/electrode contact surface (m²/m²)	Electrolyte/gas contact surface (m²/m²)	Electrode/gas contact surface (m²/m²)
sp	1.2×10^6	0.64	0.36	0.8
g	$1.4 \times 10^{3*}$	0.64	0.96	1.6
Ratio $\frac{g}{sp}$	860	16	0.38	0.50

* Determined from the circumference of the oval flattened parts of the electrode.

Downloaded 22 Jun 2009 to 130.89.112.86. Redistribution subject to ECS license or copyright; see http://www.ecsdl.org/terms_use.jsp

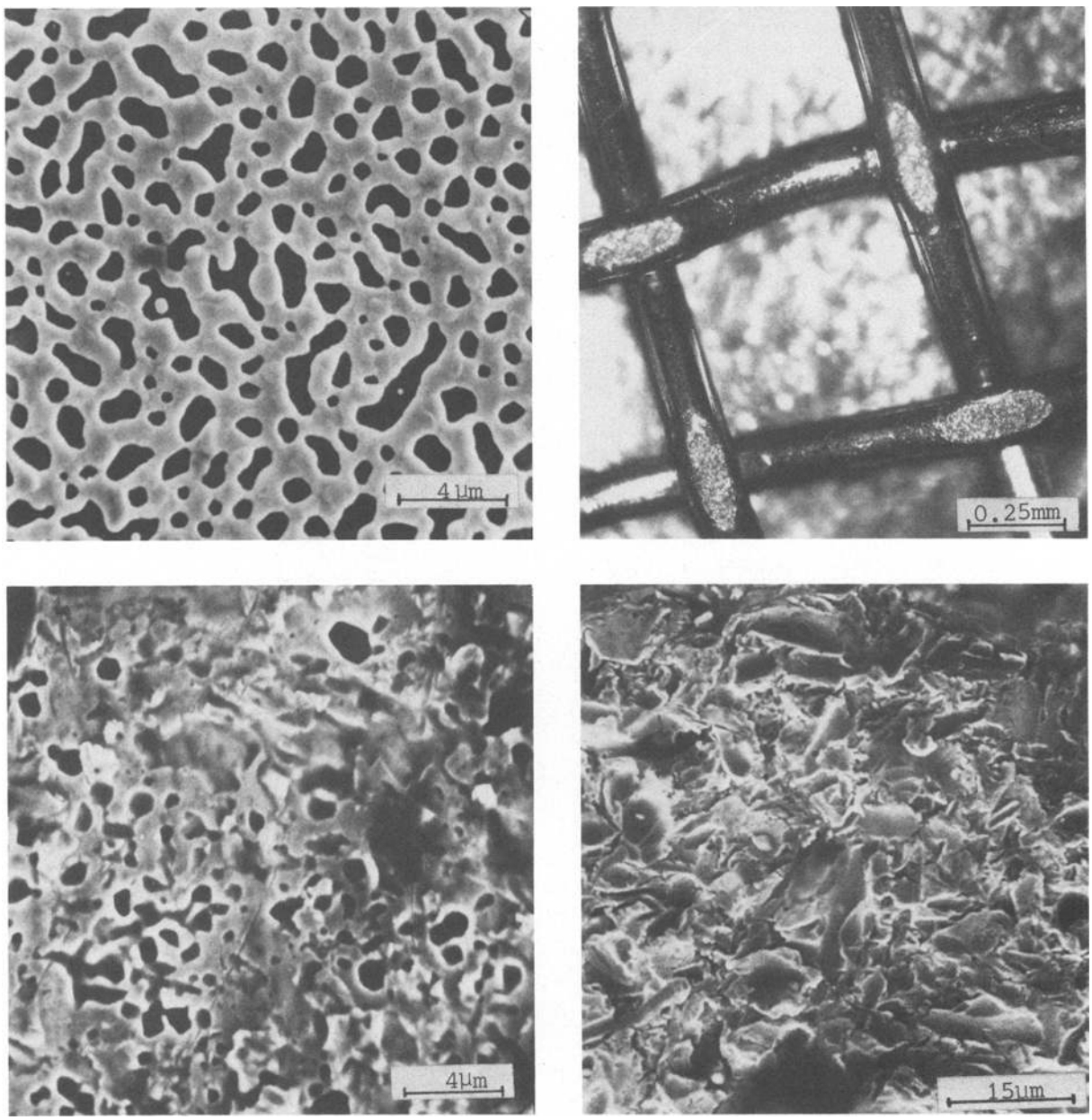

Fig. 2. Morphology of the platinum electrodes used in this study. Sputtered electrode (a, upper left), gauze electrode (b, upper right), contact surface of a gauze electrode after use on a ZY17 or CG10 sample (c, lower left), and contact surfaces of a gauze electrode after use on a BE20, BE30, or BE40 sample (d, lower right).

The elementary adsorption step in the electrode process is given by

$$O_2(g) + 2V_{ads} \leftrightarrows 2\,O_{ads} \qquad [2]$$

where V_{ads} is a vacant adsorption site and O_{ads} is an adsorbed oxygen atom. The mass action relation for this reaction can be written as (Langmuir adsorption)

$$\theta_{ads}/(1 - \theta_{ads}) = K_1(T) \times [P_{O_2}]^{1/2} \qquad [3]$$

The equilibrium constant is given by

$$K_1(T) = K_1^{o} \exp(\Delta H_{ads}/RT) \qquad [4]$$

where ΔH_{ads} is the heat of adsorption.

The adsorption step is followed by diffusion to the reaction site

$$O_{ads} + V_{rs} \leftrightarrows O_{rs} + V_{ads} \qquad [5]$$

where V_{rs} and O_{rs} are a vacant and occupied reaction site, respectively.

At the reaction site the charge transfer process takes place (given in Kröger-Vink notation)

$$O_{rs} + 2e' + V_O^{\cdot\cdot} \rightleftarrows O_O^{x} + V_{rs} \qquad [6]$$

If the charge process is rate limiting the relation between the current I and the overpotential η is given by the Butler-Volmer equation (17)

$$I = I_o[\exp(\alpha_a n V^*) - \exp(-\alpha_c n V^*)] \qquad [7]$$

$$V^* = \eta \mathbf{F}/RT \qquad [8]$$

where α_a and α_c are the anodic and cathodic transfer coefficients, respectively, V^* is a dimensionless potential, I_o the exchange current, and n number of charges transferred.

However, if the anodic or cathodic process is limited by mass transport the following equation holds (17)

$$I = [\exp(\alpha_a n V^*) - \exp(-\alpha_c n V^*)]/$$
$$[I_o^{-1} + I_{la}^{-1} \exp(\alpha_a n V^*) + I_{lc}^{-1} \exp(-\alpha_c n V^*)] \qquad [9]$$

where I_{la} and I_{lc} are the anodic and cathodic limiting current, respectively, and are defined positive. At low overpotentials, $|nV^*| << 1$, ohmic behavior is obtained

$$I = nV^*/(I_o^{-1} + I_{la}^{-1} + I_{lc}^{-1}) \qquad [10]$$

Using [8] we find

Downloaded 22 Jun 2009 to 130.89.112.86. Redistribution subject to ECS license or copyright; see http://www.ecsdl.org/terms_use.jsp

$$R_{el} = \frac{\eta}{I} = R_{ct} + R_{la} + R_{lc} \quad [11]$$

with $R_{ct} = \frac{RT}{nF} \cdot \frac{1}{I_o}$, $R_{la} = \frac{RT}{nF} \cdot \frac{1}{I_{la}}$, and $R_{lc} = \frac{RT}{nF} \cdot \frac{1}{I_{lc}}$.

From Eq. [9]-[11] it is clear that for I_{la}, $I_{lc} >> I_o$ the electrode process is determined by the charge transfer and for $I_o >> I_{la}$, I_{lc} by mass transport.

The oxygen atoms for the electrode process can be supplied by dissociated adsorption of oxygen molecules at the electrode or the electrolyte and the charge transfer will take place near the triple line (this will be further discussed below). Now we assume a model where the limiting current originates from diffusion of atomic oxygen from the adsorption site at $x = \delta$ to the reaction site at $x = 0$. At $x = \delta$ the concentration oxygen atoms is constant [see part II of this study (12)]. We can write then for I_c and I_a

$$I_c = -D_o nF \frac{C_o(\text{ads}) - C_o(\text{rs})}{\delta'} \quad [12]$$

$$I_a = D_o nF \frac{C_o(\text{rs}) - C_o(\text{ads})}{\delta''} \quad [13]$$

where D_o and C_o are the diffusion coefficient and the concentration of the oxygen atoms. I_c and I_a are given per surface unit of reaction area. A cathodic and anodic limiting current is observed for $C_o(\text{rs}) \rightarrow 0$ and $C_o(\text{rs}) \rightarrow C_o'(\text{rs})$, respectively, and are given by

$$I_{lc} = D_o nF \frac{C_o(\text{ads})}{\delta'} \quad [14]$$

$$I_{la} = D_o nF \frac{C_o'(\text{rs}) - C_o(\text{ads})}{\delta''} \quad [15]$$

where $C_o'(\text{rs})$ is the surface concentration of oxygen atoms for $\theta = 1$.

Results and Discussion

Pt electrodes on ZY17.—For all samples the I-V relation at small voltages shows an ohmic behavior, as shown in Fig. 3 for ZY17. Due to a small d-c voltage of 0-1 mV, probably originating from thermoelectric effects, the curves do not pass through the origin. The determination of the electrode resistance according to Eq. [1] is not influenced by this small voltage.

The electrode resistance R_{el} measured as a function of temperature for P_{O_2} is equal to 1, 0.21, 1.6×10^{-2}, and 9×10^{-4} atm O_2, respectively. Values of the activation energy E_a and the pre-exponential term log R_o are given in Table III. The results for a sputtered and a gauze electrode at $P_{O_2} = 1.6 \times 10^{-2}$ atm are shown

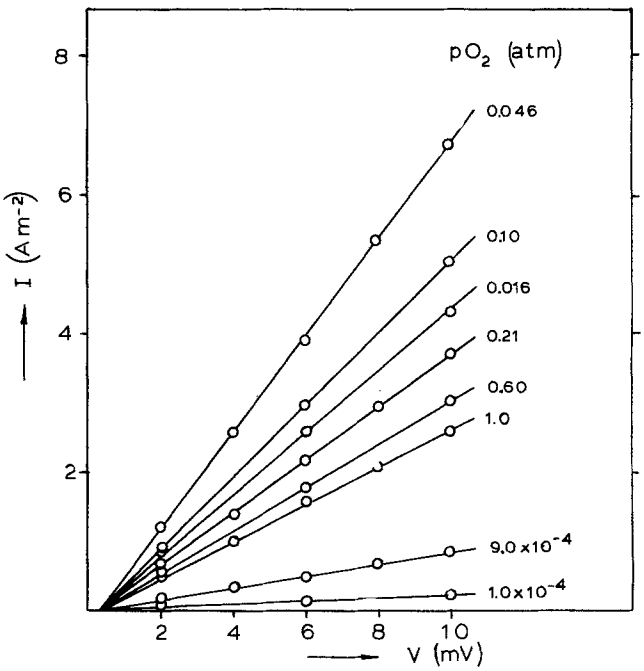

Fig. 3. Current-voltage characteristics for ZY17 at $T = 983$ K using Pt-sputtered electrodes.

in Fig. 4. At about 960 K a bend in the Arrhenius plot of R_{el} is observed and E_a changes from about 75 kJ mol^{-1} (high temperature part) to about 250 kJ mol^{-1} (low temperature part). This bend is correlated with a change from the regime where $R_{el} \sim P_{O_2}^{-1/2}$ to the regime where $R_{el} \sim P_{O_2}^{+1/2}$ (see below). Its position on the temperature scale depends on the P_{O_2} pressure and its position on the P_{O_2} scale on the temperature (Fig. 5).

Figure 5a gives R_{el} as a function of P_{O_2} at 983 K. For comparison the R_{el}-P_{O_2} relation calculated from Table III for 908 K is also given in this figure. A minimum in the R_{el}-P_{O_2} curve is observed at a value of $P_{O_2}^{\text{min.}}$. For both sputtered and gauze electrodes at $P_{O_2} < P_{O_2}^{\text{min.}}$ one finds $R_{el} \sim P_{O_2}^{-1/2}$ and from Fig. 4 and Table III it follows that in this region E_a has a value of 75-100 kJ mol^{-1}. Whereas $P_{O_2} > P_{O_2}^{\text{min.}}$ one finds $R_{el} \sim P_{O_2}^{+1/2}$ and in this region E_a has a value of about 250 kJ mol^{-1}. The value of $P_{O_2}^{\text{min.}}$ shifts to higher values with increasing temperature.

These results are in good agreement with literature data concerning platinum electrodes on stabilized zirconia. However, the reported experimental literature data are incomplete and only parts of the picture described above were measured. A minimum in the

Table III. Activation energies and log R_o of the electrode resistance of sputtered (sp) and gauze (g) electrodes on several electrolytes. The deviation is given in the 65% reliability interval.

	1 atm O_2		0.21 atm O_2		1.6×10^{-2} atm O_2			9×10^{-4} atm O_2		
System	$-\log R_o$ (Ωm^2)	E_a (kJ mol^{-1})	$-\log R_o$ (Ωm^2)	E_a (kJ mol^{-1})	Range (K)	$-\log R_o$ (Ωm^2)	E_a (kJ mol^{-1})	Range (K)	$-\log R_o$ (Ωm^2)	E_a (kJ mol^{-1})
ZY17 (sp)	16.9 ± 0.9	270 ± 15	16.5 ± 0.4	260 ± 7	<970	15.3 ± 0.6	230 ± 10	<925	9.8 ± 0.5	145 ± 10
					>970	6.6 ± 0.6	72 ± 10	>925	5.6 ± 0.5	70 ± 10
ZY17 (g)	13.8 ± 0.6	245 ± 10	15.8 ± 0.7	280 ± 10	<960	9.9	167		5.5 ± 0.1	98 ± 5
					>960	4.9 ± 0.4	75 ± 10			
CG10 (sp)	14.8 ± 0.5	230 ± 10	14.9 ± 0.5	321 ± 9	<970	16.0 ± 0.1	245 ± 3	<930	10.3 ± 0.1	148 ± 1
					>970	7.7 ± 0.3	91 ± 6	>930	5.4 ± 0.3	61 ± 4
CG10 (g)	12.3 ± 0.3	212 ± 6	12.3 ± 0.3	208 ± 6	<940	12.1	203		5.5 ± 0.2	96 ± 4
					>940	5.1 ± 0.3	77 ± 5			
									2.2 × 10^{-4} atm O_2	
BE20 (sp)	11.8 ± 0.4	145 ± 6	9.6 ± 0.1	115 ± 2		10.0 ± 0.3	129 ± 5		7.1 ± 0.3	101 ± 6
BE20 (g)	9.7 ± 0.3	133 ± 5	9.8 ± 0.4	137 ± 7		8.1 ± 0.4	116 ± 6		5.6 ± 0.6	83 ± 10
BE30 (sp)	11.1 ± 0.1	138 ± 2	10.0 ± 0.3	125 ± 5		9.2 ± 0.2	121 ± 3		6.8 ± 0.6	99 ± 10
BE30 (g)	8.3 ± 0.3	112 ± 5	7.9 ± 0.4	108 ± 6		6.3 ± 0.3	87 ± 4		3.4 ± 0.4	45 ± 7
BE40 (sp)	10.3 ± 0.4	129 ± 7	8.8 ± 0.5	110 ± 8		9.6 ± 0.3	125 ± 5		5.7 ± 1.1	75 ± 20
BE40 (g)	8.3 ± 0.4	119 ± 7	7.7 ± 0.5	110 ± 8		6.9 ± 0.2	102 ± 3		3.3 ± 0.3	45 ± 6
BE20 (gold, sp)			11.2 ± 0.9	150 ± 15						

Downloaded 22 Jun 2009 to 130.89.112.86. Redistribution subject to ECS license or copyright; see http://www.ecsdl.org/terms_use.jsp

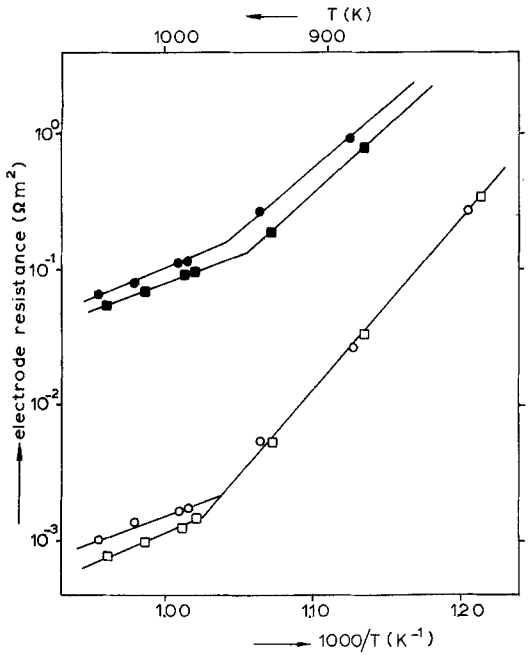

Fig. 4. Electrode resistance as a function of temperature for $P_{O_2} = 1.6 \times 10^{-2}$ atm O_2. ○, Pt-sputtered electrode on ZY17; ●, Pt-gauze electrode on ZY17; □, Pt-sputtered electrode on CG10; ■, Pt-gauze electrode on CG10.

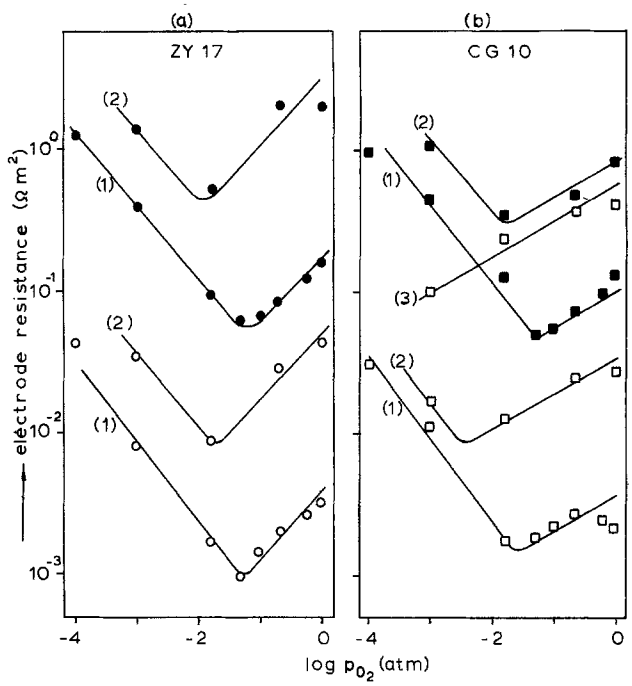

Fig. 5. (a) Electrode resistance as a function of the oxygen partial pressure at 983 K, 1; 908 K, 2; and 833 K, 3. Pt electrodes on ZY17. The drawn lines represent a $P_{O_2}^{-1/2}$ and $P_{O_2}^{+1/2}$ dependence respectively. (b) Pt electrodes on CG10. The drawn lines represent a $P_{O_2}^{-1/2}$ and $P_{O_2}^{+1/4}$ dependence respectively. Open points: sputtered electrodes. Closed points: gauze electrodes.

R_{el}-P_{O_2} curve was reported by Schouler (4) for Pt-sputtered and Pt-paste electrodes on $(ZrO_2)_{0.83}(YO_{1.5})_{0.17}$ and by Hartung (6) for Pt-paste electrodes on $(ZrO_2)_{0.82}(YO_{1.5})_{0.10}(MgO)_{0.08}$. According to Bauerle (2) at 1073 K, $R_{el} \sim P_{O_2}^{-0.64}$ at low oxygen partial pressures and becomes constant at high oxygen partial pressures (0.21-1.00 atm O_2) for Pt-sputtered electrodes on yttria-stabilized zirconia (YSZ). In the opinion of the authors the experimental data permit the following interpretation: $P_{O_2}^{min.}$ has a value of 0.21-1.00 atm O_2 and for $P_{O_2} < P_{O_2}^{min.}$ $R_{el} \sim P_{O_2}^{-0.5}$. For Pt electrodes on YSZ an activation energy of about 100 kJ mol^{-1} was reported in Ref. (4 and 7) in the region where $R_{el} \sim P_{O_2}^{-1/2}$ and a value of about 250 kJ mol^{-1} in Ref. (2 and 4) in the region where $P_{O_2} > P_{O_2}^{min.}$.

The observed phenomena were ascribed by Schouler (4) to oxidation of the platinum surface. This hypothesis may be a good explanation for the high activation energy found at high P_{O_2}. The observed relationship $R_{el} \sim P_{O_2}^{+1/2}$ at $P_{O_2} > P_{O_2}^{min.}$ cannot be explained with the formation of an oxidized Pt surface because it is well known that this is catalytically less active.

In our opinion the observed phenomena can be explained in the following way. The oxygen atoms for the electrode process are supplied by dissociative adsorption of oxygen molecules at the Pt electrode. The overall electrode reaction is rate determined by diffusion of the oxygen atoms from the adsorption site to the reaction side (see section on Theory). At $P_{O_2} < P_{O_2}^{min.}$, θ_{ads} is low and mass transport limitation occurs at the cathode. At $P_{O_2} > P_{O_2}^{min.}$, $\theta_{ads} \approx 1$ and mass transport limitation occurs at the anode. This hypothesis is discussed in the following.

As shown by Wang and Nowick (5) the electrode resistance varies as the $-1/4$ or $+1/4$ power of P_{O_2} if the electrode process is determined by charge transfer (see following section). The experimentally found powers of $-1/2$ and $+1/2$ point to mass transfer limitation and can be derived from Eq. [14] and [15]. For $\theta_{ads} << 1$ holds $(1 - \theta_{ads}) \approx 1$ and assuming that $\delta' \approx \delta''$ we find $I_{1a} >> I_{1c}$. From Eq. [3] it follows that $\theta_{ads} = K_1(T) \times [P_{O_2}]^{1/2}$ and using Eq. [10], [11], and [14] it is found that

$$R_{el} = R_{1c} \sim \frac{\delta}{D_o\sqrt{K_1}} P_{O_2}^{-1/2} \qquad [16]$$

For $\theta_{ads} \approx 1$ we find that $I_{1c} >> I_{1a}$ and $(1 - \theta_{ads}) = K_1(T) \times [P_{O_2}]^{-1/2}$ and this results in

$$R_{el} = R_{1a} \sim \frac{\delta\sqrt{K_1}}{D_o} P_{O_2}^{+1/2} \qquad [17]$$

According to Eq. [16] at $P_{O_2} < P_{O_2}^{min.}$ (*i.e.*, $\theta_{ads} << 1$) mass transport limitation of oxygen atoms occurs at the cathode and according to Eq. [17] at $P_{O_2} > P_{O_2}^{min.}$ (*i.e.*, $\theta_{ads} \approx 1$) mass transport limitation of oxygen atoms occurs at the anode. The surface coverage of oxygen atoms decreases with increasing temperature and this is in a good agreement with the observed change of $P_{O_2}^{min.}$ as a function of T. From Eq. [16] and [17] it follows that in the region where R_{el} varies with $P_{O_2}^{-1/2}$ and $P_{O_2}^{+1/2}$ the activation energy of R_{el} is given by $E_a(R_{el}) = \Delta H_d - 1/2\Delta H_{ads}$ and $E_a(R_{el}) = \Delta H_d + 1/2\Delta H_{ads}$, respectively, where ΔH_d is the activation enthalpy for diffusion. In literature no precise data are known of ΔH_d and ΔH_{ads} as a function of the coverage. Supposing that ΔH_d and ΔH_{ads} are not strongly dependent on the coverage, we calculate from the experimental values of $E_a(R_{el})$ for ΔH_d and ΔH_{ads} values of 170 and 160 kJ mol^{-1}, respectively. These calculated data are in reasonable agreement with literature data concerning ΔH_d and ΔH_{ads} of oxygen on platinum. Lewis and Gomer (19) found a surface diffusion enthalpy of 145 kJ mol^{-1} for oxygen atoms on platinum at $T >$ 500 K. The values of the enthalpy of adsorption found by different authors scatter. Brennan *et al.* (21) reported that ΔH_{ads} decreases with increasing surface coverage from 285 to 150 kJ mol^{-1} (300 K). Netzer and Gruber (18) reported for high surface coverages a value for ΔH_{ads} of 135 kJ mol^{-1} (670-770 K). Finally, ΔH_{ads} can be calculated from the temperature dependence of $P_{O_2}^{min.}$. According to the Langmuir equation a minimum in R_{el} is predicted for $\theta = 1/2$ and with Eq. [3] this results in $K_1(T) \times P_{O_2}^{min.} = 1$. From Schouler's (4) data it follows that $\Delta H_{ads} = 280 \pm 15$ kJ mol^{-1} and from our data $\Delta H_{ads} = 160 \pm 30$ kJ mol^{-1}.

Downloaded 22 Jun 2009 to 130.89.112.86. Redistribution subject to ECS license or copyright; see http://www.ecsdl.org/terms_use.jsp

Additional evidence that the oxygen atoms for the electrode process are supplied by dissociative adsorption on the Pt electrode and not on the electrolyte comes from the following data. First, $P_{O_2}^{min.}$ has about the same value for Pt electrodes on ZY17 and on CG10 (compare Fig. 5a and b) while with other electrode materials no $P_{O_2}^{min.}$ is observed and E_a has a quite different value (4, 9). Finally, the work of Kleitz (8) strongly suggests that adsorbed oxygen atoms on the stabilized zirconia surface are practically immobile.

The proposed hypothesis for the mechanism of the electrode reaction on ZY17 gives a good explanation for the limiting current observed by Gür (20) at low voltages ($\leq$ 300 mV). Gür performed measurements on the cell

$$(-)P_{O_2}, Pt|ZrO_2 - Sc_2O_3|Pt, air\ (+)$$

in the temperature region of 873-1173 K and P_{O_2} region of 10^{-6}-1 atm. The limiting current was observed below 1073 K and was independent of the oxygen partial pressure at the cathode. Gür (20) assumed that the anodic polarization of the cell was negligible. However, as discussed above, at $T < 1073$ K, $\theta_{ads} \approx 1$ in air. At a high surface coverage of oxygen atoms the electrode process is limited by mass transport at the anode, see Eq. [15]. According to Gür (20) the limiting current has an activation energy of about 250 kJ mol^{-1} and this value is in a good agreement with the value found in this study for $E_a(R_{el})$ at $\theta_{ads} \approx 1$. Therefore, we can conclude that the limiting current at these high P_{O_2} values and low temperatures has to be correlated with mass transport limitation at the anode.

The location of the reaction site is discussed in the following. The difference in electrode resistance between a gauze and sputtered electrode ($R_{el}(g)/R_{el}(sp) \approx 50$) cannot be simply correlated with the size of the electrolyte/electrode two-phase area or the length of the three-phase line. An additional experiment was performed to determine whether the size of the electrolyte/electrode two-phase area or the length of the three-phase line plays a role in the magnitude of R_{el}. On three identical samples a 0.3 μm thick Pt electrode was sputtered and subjected to different thermal treatments resulting in strongly different electrode morphologies. The characteristic data are summarized in Table IV. The shape of the frequency dispersion diagrams is not influenced by the size of the Pt grains. This is a strong indication that the mechanism of the electrode process is not influenced by the particle size of the Pt grains. As shown in Table IV the electrode resistance increases strongly with increasing particle size. With increasing particle size the size of the electrolyte/electrode two-phase area is nearly constant whereas the length of the three-phase line decreases. We can conclude that the reaction area is correlated with the length of the three-phase line. The width of the three-phase line area (perpendicular on this line) is small in comparison with the smallest Pt particles used.

Pt electrodes on CG10.—The data of sputtered and gauze electrodes on CG10 are summarized in Fig. 4 and 5 and in Table III. The characteristics of Pt electrodes on CG10 show a large similarity with that of Pt electrodes on ZY17 and are therefore briefly discussed.

Table IV. Characteristic data of a Pt-sputtered electrode on ZY17, treated at different temperatures

Thermal treatment temperature (K)	Size of the Pt-grains (μm)	Length of the three-phase line (m/m^2)	Electrolyte/electrode contact surface (m^2/m^2)	Electrode resistance (O_2, 823K) (Ωm^2)
973	$\leq$0.1	$\geq 1.5 \times 10^7$	0.99	0.95
1173	0.5	3×10^6	0.93	6.25
1273	1.0	1.5×10^6	0.85	10.5

In the R_{el}-P_{O_2} relation a minimum is observed. For $P_{O_2} > P_{O_2}^{min.}$ it is found that $R_{el} \sim P_{O_2}^{1/4}$ and $E_a(R_{el}) \approx 230$ kJ mol^{-1}, whereas in the region where $P_{O_2} < P_{O_2}^{min.}$, $R_{el} \sim P_{O_2}^{-1/2}$ and $E_a(R_{el}) \approx$ 75-100 kJ mol^{-1}.

In the region of $P_{O_2} > P_{O_2}^{min.}$ there is a good agreement with the data of Wang and Nowick (5) for Pt-paste electrodes on CeO_2-CaO [1-15 mol percent (m/o)] and CeO_2-Y_2O_3 (6 m/o). The power 1/4 points to charge transfer limitation, as shown by Wang and Nowick (5). The exchange current is given by

$$I_o \sim K_{ct}[\theta(1-\theta)]^{1/2} \quad [18]$$

where K_{ct} is the charge transfer reaction constant. If the electrode reaction is determined by the charge transfer and the oxygen for this process is supplied through adsorbed oxygen atoms on the electrode, it is derived from Eq. [3], [10], and [18] that for $P_{O_2} > P_{O_2}^{min.}$ (*i.e.*, $\theta \approx 1$) $R_{ct} \sim P_{O_2}^{+1/4}$. The activation energy is given by $E_a(R_{el}) = E_a(ct) + \Delta H_{ads}/4$ (5), where $E_a(ct)$ is the activation energy of the charge transfer. Using the experimental values $E_a(R_{el})$ and $\Delta H_{ads} =$ 160 kJ mol^{-1} the value of $E_a(ct)$ is calculated to be 190 kJ mol^{-1}.

In the region of $P_{O_2} < P_{O_2}^{min.}$ Wang and Nowick (5) found that $R_{el} \sim P_{O_2}^{-1/4}$ and $E_a(R_{el}) \approx 95$ kJ mol^{-1}. The power $-1/4$ can be derived from Eq. [3], [10], and [18] assuming that the electrode process is determined by the charge transfer and $\theta << 1$ (5). However, in this study we found that $R_{el} \sim P_{O_2}^{-1/2}$, pointing to mass transport limitation. In our opinion this difference can be explained in the following way. For ceria-based materials with a porous electrode I_o is of the same order of magnitude as I_{lc}. Depending on the electrode morphology, the electrode process will be dominated by I_o or I_{lc}. The electrodes studied by Wang and Nowick (5) have larger metal grain sizes than used in this study. The influence of the morphology of the Pt electrode is clearly illustrated by the fact that for Pt foil electrodes on substituted ceria diffusion along the electrolyte/electrode interphase is rate determining, as shown by Wang and Nowick (9).

Pt electrodes on BE20, BE30, and BE40.—The electrode resistance of a Pt-sputtered and Pt-gauze electrode on BE20, BE30, and BE40 was measured as a function of T in the oxygen partial pressure range 1.0-2.2 $\times$ 10^{-4} atm O_2. Values of $E_a(R_{el})$ and log R_o are given in Table III. Figure 6 gives R_{el} for sputtered and gauze electrodes as a function of temperature. The electrode resistance increases with increasing Er content. $E_a(R_{el})$ for sputtered and gauze electrodes has a value of about 125 kJ mol^{-1} in the region of $P_{O_2} =$ 1-1.6 $\times$ 10^{-2} atm O_2 and is independent of the Er content. For $P_{O_2} = 2.2 \times 10^{-4}$ atm, $E_a(R_{el})$ varies in the region of 50-100 kJ mol^{-1}.

$E_a(R_{el})$ is slightly higher than the activation energy of the bulk conductivity at $T < 820$ K [$E_a(b) \approx 115$ kJ mol^{-1}] and both the bulk and electrode resistance increase with increasing Er content. Yet, the electrode resistance cannot be directly correlated with bulk effects. For the sample BE20 $E_a(b)$ changes at 870 K from 115 kJ mol^{-1} (low temperature part) to 62 kJ mol^{-1} (high temperature part) and this change is not reflected in the R_{el}-T^{-1} curve.

Figure 7 gives the electrode resistance of sputtered and gauze electrodes on BE20 and BE40 as a function of P_{O_2} (the values for BE30 are omitted for clarity reasons). For sputtered electrodes the relation $R_{el} \sim P_{O_2}^{-1/2}$ is found, pointing to mass transport of atomic oxygen as the rate-limiting step (see section on Pt electrodes on ZY17). For gauze electrodes the relation $R_{el} \sim P_{O_2}^{-3/8}$ is found. As shown by Wang and Nowick (9) the 3/8 power can be derived if the charge transfer takes place on the electrolyte/electrode interface and diffusion along this interface is rate determining. As shown in part II of this study (12), R_{el} consists of a parallel combination of two resistances. Therefore, in

Downloaded 22 Jun 2009 to 130.89.112.86. Redistribution subject to ECS license or copyright; see http://www.ecsdl.org/terms_use.jsp

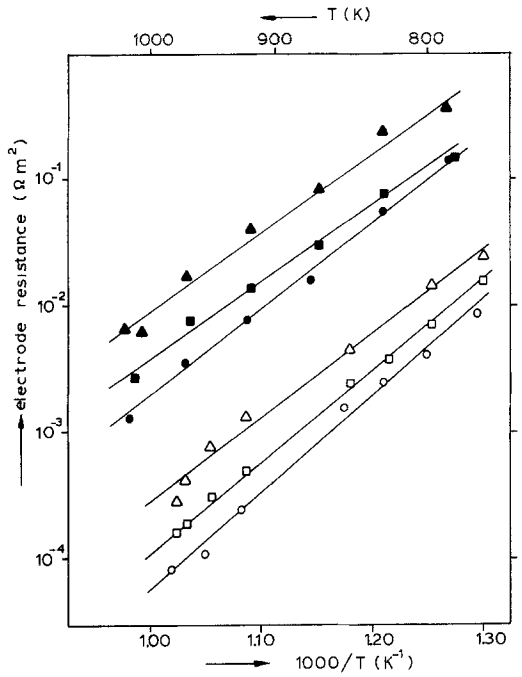

Fig. 6. Electrode resistance of platinum electrodes on BE20 (circles), BE30 (squares), and BE40 (triangles) as a function of the temperature in O_2 (1 atm). Open points: sputtered electrodes. Closed points: gauze electrodes.

this case the observed P_{O_2} dependency is the result of two other dependencies. This will be further discussed in part II (12).

In contrast with the data for Pt electrodes on ZY17 and CG10 (see Fig. 5) no minimum in the R_{el}-P_{O_2} relation for Pt electrodes on Bi_2O_3-based materials is observed (see Fig. 7). In the section on Pt electrodes on ZY17 it was concluded that for ZY17 and CG10 the oxygen atoms for the electrode process are supplied by dissociative adsorption of oxygen molecules on the Pt electrode. Therefore, we must conclude that for the Bi_2O_3-based materials this adsorption step on Pt does not play a dominant role here. This conclusion is supported by the magnitude of $E_a(R_{el})$ on Bi_2O_3-based materials, which strongly deviates from what one expects for adsorption and diffusion on Pt. Consequently, adsorption and diffusion on the electrolyte plays a dominant role on Bi_2O_3-based materials. Additional evidence comes from the observation that $E_a(R_{el})$ is not or only slightly changed if a gold-sputtered electrode is used on BE20 (see Table III) whereas for gold electrodes on zirconia- and ceria-based materials $E_a(R_{el})$ is significantly higher (4, 9). The active site for this adsorption is probably correlated with the Bi^{3+} ion, because with decreasing amount of Bi^{3+} ions the amount of adsorption sites decreases, which results in a higher electrode resistance (it is assumed, see above, that the increased bulk electrolyte resistance does not play an important role).

The electrode resistance of a sputtered electrode on Bi_2O_3-based materials is 10-30 times lower than that of a gauze electrode. This suggests that the charge transfer takes place on the electrolyte/electrode interface (see Table II). However, due to the fact that it is questionable whether the electrode mechanism is the same for a sputtered and gauze electrode, these data are not further used to determine the reaction site.

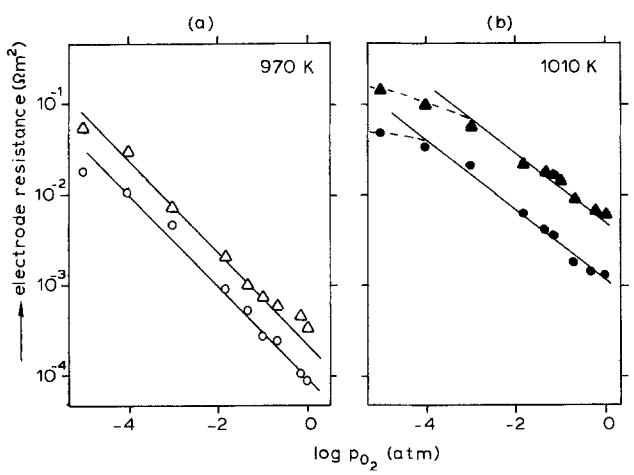

Fig. 7. Electrode resistance of Pt-sputtered electrodes (a) and Pt-gauze electrodes (b) as a function of the oxygen partial pressure. In (a) the drawn lines represent a $P_{O_2}^{-1/2}$ dependence and in (b) a $P_{O_2}^{-3/8}$ dependence. BE20: circles. BE40: squares.

Comparison of the Different Electrolytes

The combination of the electrolyte material, electrode material, and electrode morphology determines whether the dominating adsorption, dissociation, or diffusion step takes place at the electrolyte, electrode, or at the electrolyte/electrode interface. As shown above, there are large differences between the adsorption behavior of, on the one hand, ZY17 and CG10 and, on the other hand, the electrolytes BE20, BE30, and BE40, both groups in combination with porous Pt electrodes. In case of ZY17 and CG10 the oxygen atoms for the electrode process are supplied by the platinum electrode, whereas for the Bi_2O_3-based materials the oxygen atoms are supplied by the electrolyte surface. Therefore, it can be expected that there are large differences in the polarization of Pt electrodes on ZY17 and CG10, on the one hand, and Bi_2O_3-based materials, on the other hand.

Table V summarizes the values of the electrode resistance for Pt-sputtered and Pt-gauze electrodes on several electrolytes. The data for $P_{O_2} = 1$ atm lie in the region where θ_{ads} on Pt is about one and the data for $P_{O_2} = 9 \times 10^{-4}$ atm O_2 in the region where θ_{ads} (Pt) $<< 1$. As expected, the electrode resistance for Pt electrodes on ZY17 and CG10 is similar. However, the electrode resistance for Pt electrodes on Bi_2O_3-based materials is much smaller. In the region where θ_{ads}(Pt) $<< 1$ the resistance of sputtered and gauze electrodes on BE20 is respectively 4 and 20 times smaller than that of similar electrodes on ZY17.[2] In the region where θ_{ads}(Pt) ≈ 1 the electrode resistance on BE20 at 974 K is 40 (sputtered electrode) and 80 (gauze electrode) times smaller than on ZY17 and at 873 K these values are 250 and 400 times smaller, respectively. These data show clearly the influence of the electrolyte on the electrode resistance of Pt/Bi_2O_3-

[2] It must be noticed that the microscopic structure of a gauze electrode on ZY17, CG10, and on BE20, 30, 40 differ (see section on Electrode Preparation and Characterization).

Table V. Electrode resistance for platinum-sputtered electrodes (sp) and platinum-gauze electrodes (g) on several electrolytes

System	Electrode resistance (10^{-3} Ωm²) 1 atm O_2 873 K	1 atm O_2 973 K	9×10^{-4} atm O_2 973 K
ZY17 (sp)	184	4.1	14.5
CG10 (sp)	93	3.7	7.6
BE20 (sp)	0.76	0.098	3.9
BE30 (sp)	1.43	0.20	5.5
BE40 (sp)	2.65	0.43	6.7
ZY17 (g)	7370	230	550
CG10 (g)	2470	125	460
BE20 (g)	18.3	2.8	22*
BE30 (g)	25.6	5.2	44*
BE40 (g)	66.7	12	95*

* These values were calculated from the R_{el}-P_{O_2} plot at 1073 K shown in Fig. 7b, assuming E_a = 120 kJ mol⁻¹.

Downloaded 22 Jun 2009 to 130.89.112.86. Redistribution subject to ECS license or copyright; see http://www.ecsdl.org/terms_use.jsp

based systems, an effect which becomes larger with increasing P_{O_2} and lower temperatures.

For Pt electrodes with the same morphology, at $P_{O_2} > P_{O_2}^{min.}$ the electrode process on ZY17 is determined by mass transfer (see section on Pt electrodes on ZY17), whereas for CG10 by charge transfer (see section on Pt electrodes on CG10). Due to a similar electrode morphology I_{la} will have the same value for CG10 and ZY17 and therefore we can conclude that on CG10 I_o is smaller (and becomes rate determining) than on ZY17.

Oxygen ion conductors may be used in devices in which pumping of oxygen plays an important role, *i.e.*, oxygen pumps for the enrichment of air. For comparing the different materials as a potential candidate for the solid electrolyte, current-overpotential relations for Pt electrodes were measured in air. The results for sputtered and gauze electrodes are shown in Fig. 8a and b.[3] The current that can be drawn at $\eta = 600$ mV is for BE20 using sputtered electrodes about 5 times higher than for ZY17 and for gauze electrodes about 10 times higher. This shows that the Bi_2O_3-based materials are superior to the other materials with respect to its electrochemical characteristics. For a better understanding of these current-overvoltage curves, the anodic and cathodic contributions to the polarization have to be separated by using a reference electrode.

[3] Remark that Fig. 8 cannot be calculated from Fig. 5 due to different experimental conditions (Fig. 8: high voltage/currents resulting in different electrode morphology and additional processes).

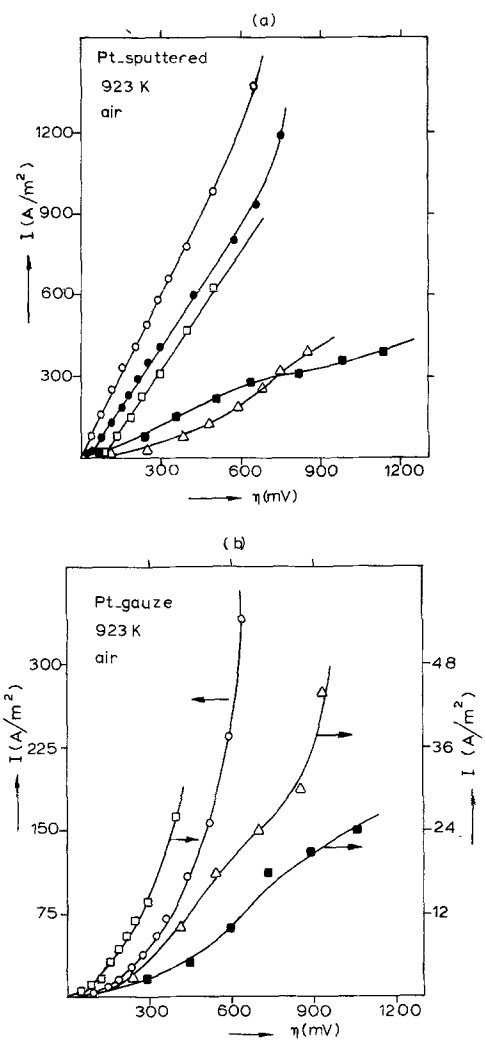

Fig. 8. Current-overvoltage curves for Pt-sputtered electrodes (a) and Pt-gauze electrodes (b) for several electrolytes in air at 923 K. ○, BE20; ●, BE30; □, BE40; ■, ZY17; △, CG10.

Conclusions

1. The combination of electrolyte and electrode material determines whether the dominating adsorption or diffusion step takes place on the electrolyte or on the electrode.

2. For ZY17 and CG10 the oxygen atoms for the electrode process are supplied by dissociative adsorption of oxygen molecules on the Pt electrode. For low temperatures and high oxygen partial pressures the surface coverage of oxygen atoms on the Pt electrode is about one and in this region we find that $R_{el} \sim P_{O_2}{}^{+n}$. For ZY17 mass transport at the anode is rate determining ($n = ½$) and for CG10 the charge transfer ($n = ¼$). If the surface coverage of oxygen atoms on the electrode is low we find for ZY17 and CG10 that $R_{el} \sim P_{O_2}{}^{-½}$, showing that mass transport of atomic oxygen at the cathode is rate determining.

3. For Bi_2O_3-based materials adsorption and diffusion on the solid electrolyte determines the behavior of R_{el}. The electrode process is determined by mass transport at the cathode. The electrode resistance increases with increasing amount of substituent.

4. The electrode resistance for electrodes with the same morphology is for Bi_2O_3-based materials many times lower than for materials based on ZrO_2 and CeO_2.

Acknowledgments

We would like to thank Mr. J. M. Paauwe for experimental assistance and Dr. K. J. de Vries and Mr. H. Kruidhof for supplying the CeO_2-Gd_2O_3 sample. Financial assistance from Philips N. V. (Elcoma) is gratefully acknowledged.

Manuscript submitted Jan. 27, 1982; revised manuscript received July 20, 1982.

Any discussion of this paper will appear in a Discussion Section to be published in the December 1983 JOURNAL. All discussions for the December 1983 Discussion Section should be submitted by Aug. 1, 1983.

Publication costs of this article were assisted by the Twente University of Technology.

REFERENCES

1. R. J. Brook, W. L. Peltzmann, and F. A. Kröger, *This Journal*, **118**, 185 (1971).
2. J. E. Bauerle, *J. Phys. Chem. Solids*, **30**, 2657 (1969).
3. S. V. Karpachev and Yu Ovchinnikov, *Sov. Electrochem.*, **5**, 181 (1969).
4. E. Schouler, Ph.D. Thesis, Grenoble (1979).
5. Da Yu Wang and A. S. Nowick, *This Journal*, **126**, 1155 (1979).
6. R. Hartung, *Z. Phys. Chem.*, **260**, 259 (1979).
7. P. Fabry and M. Kleitz, *Electroanal. Chem. Interfacial Electrochem.*, **57**, 165 (1974).
8. M. Kleitz, Ph.D. Thesis, Grenoble (1968).
9. Da Yu Wang and A. S. Nowick, *This Journal*, **128**, 55 (1981).
10. M. J. Verkerk, K. Keizer, and A. J. Burggraaf, *J. Appl. Electrochem.*, **10**, 81 (1980).
11. M. J. Verkerk and A. J. Burggraaf, *This Journal*, **128**, 75 (1981).
12. M. J. Verkerk and A. J. Burggraaf, *ibid.*, **130**, 78 (1983).
13. M. J. Verkerk, B. J. Middelhuis, and A. J. Burggraaf, *Solid State Ionics*, **6**, 159 (1982).
14. M. A. C. G. van de Graaf, T. van Dijk, M. A. de Jongh, and A. J. Burggraaf, "Science of Ceramics," Vol. 9, K. J. de Vries, Editor, p. 75, Sterwin Rivers, Ltd., Cobridge, England (1977).
15. D. Yuan and F. A. Kröger, *This Journal*, **116**, 594 (1969).

Downloaded 22 Jun 2009 to 130.89.112.86. Redistribution subject to ECS license or copyright; see http://www.ecsdl.org/terms_use.jsp

16. Y. K. Agrawal, D. W. Short, R. Gruenke, and R. A. Rapp, *ibid.*, **121**, 354 (1974).
17. H. R. Thirsk and J. A. Harrison, "A Guide to the Study of Electrode Kinetics," Academic Press, London and New York (1972).
18. F. P. Netzer and H. L. Gruber, *Z. Phys. Chem. N.F.*, **85**, 159 (1973).
19. R. Lewis and R. Gomer, *Surf. Sci.*, **12**, 157 (1968).
20. T. M. Gür, I. D. Raistrick, and R. A. Huggins, *This Journal*, **127**, 2620 (1980).
21. D. Brennan, D. O. Hayward, and B. M. W. Trapwell, *Proc. R. Soc. London, Ser. A*, **256**, 81 (1960).

Oxygen Transfer on Substituted ZrO_2, Bi_2O_3, and CeO_2 Electrolytes with Platinum Electrodes

II. A-C Impedance Study

M. J. Verkerk[1] and A. J. Burggraaf

Twente University of Technology, Department of Chemical Engineering, Laboratory of Inorganic Chemistry and Materials Science, 7500 AE Enschede, The Netherlands

ABSTRACT

An equivalent electrical circuit that describes the electrode processes on different electrolytes, using porous Pt electrodes, is given. Diffusional processes are important and have to be presented by Warburg components in the circuit. The overall electrode process is rate limited by diffusion of atomic oxygen on the electrode surface for stabilized zirconia and substituted ceria (low P_{O_2}). On stabilized bismuth sesquioxide diffusion of atomic oxygen on the electrolyte surface is rate limiting at high P_{O_2} while at low P_{O_2} another process, probably diffusion of electronic species in the electrolyte, is dominant. One of these processes plays a role too on substituted ceria at high P_{O_2}, where a charge transfer process is dominant. These results are consistent with the mechanisms developed in part I of this paper.

In part I of this paper (1) a d-c study was performed on solid electrolytes based on ZrO_2, CeO_2, and Bi_2O_3 with platinum electrodes. It was concluded that for ZrO_2- and CeO_2-based materials the oxygen atoms for the electrode process are mainly supplied by dissociative adsorption of oxygen molecules at the Pt electrode, followed by transport to the reaction site where the charge transfer occurs. For Bi_2O_3-based materials the dominant adsorption and diffusion steps (in the high P_{O_2} and low temperature region) take place on the electrolyte. This different adsorption behavior is the origin of the lower electrode resistance of a Pt electrode on Bi_2O_3-based materials in comparison with that on ZrO_2- and CeO_2-based materials. Frequency dispersion analysis is a powerful tool for studying in detail the mechanism of the electrode process on these electrolytes (2-4).

Various authors studied the frequency behavior of Pt electrodes on a solid electrolyte. Generally, for Pt-paste and Pt-sputtered electrodes on stabilized zirconia the part of the frequency dispersion diagram which corresponds to the electrode process consists of a depressed semicircle (2, 5-9). This is interpreted in terms of a parallel combination of a resistance and a double layer capacity (2). A Warburg-type behavior, which is characteristic for diffusion limitation, is sometimes observed at high temperatures and low oxygen partial pressures (5, 8, 10). For Pt-paste electrodes on substituted ceria Braunshtein *et al.* (11) found that the overall process consists of a parallel combination of a resistance and a Warburg impedance. However, Wang and Nowick (12) observed for a Pt-paste electrode on substituted ceria a depressed semicircle, which interpretation is not very clear. The electrode process on (porous) Bi_2O_3 was studied using Au-paste electrodes (13, 14). The experimental results are interpreted in terms of a parallel combination of a resistance and Warburg impedances. The Warburg impedances are correlated with diffusion on the oxide surface and on the metal surface (14). These data can hardly be used for obtaining insight on the influence of the electrolyte on the electrode process because the measurements were performed under different experimental conditions and using different electrode morphologies, which are sometimes badly characterized.

The object of this paper is to study in detail the mechanism of the electrode process on different electrolytes using frequency dispersion analysis and to support the models of the electrode process developed in part I of this study. With the frequency dispersion technique an equivalent electrical circuit of the electrode process can be achieved and resolved in its components and a further insight in the influence of the electrolyte on the electrode process can be obtained.

The following systems were studied:

$(ZrO_2)_{0.83}(YO_{1.5})_{0.17}$ (ZY17),

$(CeO_2)_{0.90}(GdO_{1.5})_{0.10}$ (CG10),

$(Bi_2O_3)_{1-x}(Er_2O_3)_x$ with $x = 0.20$, 0.30, and 0.40 (BE20, BE30, and BE40). Electrodes with the same morphology were realized on these electrolytes and this morphology was preserved during the subsequent experiments. The electrode preparation and characterization is thoroughly described in part I of this study. Experimental details concerning the preparation and characterization of electrolytes and the electrical measurements are given in Ref. (1). The procedure to determine the individual components of the equivalent electrical circuit is described elsewhere (27).

Theory

In part I of this study it was concluded that the rate-limiting step in the electrode process on ZY17, CG10 ($P_{O_2} < P_{O_2}^{min.}$), BE20, BE30, and BE40 is mass transport of oxygen atoms. In this section the relevant theory for the frequency dispersion behavior of a mass transport controlled reaction is given.

When a d-c current passes through the electrolyte the oxygen atoms for the electrode process are supplied or removed by diffusion of oxygen atoms on the electrode surface and/or electrolyte surface. The oxygen atoms diffuse over a characteristic length δ from $x = \delta$ to the triple line at $x = 0$, where the charge transfer

[1] Present address: Philips Research Laboratories, Eindhoven, The Netherlands.

Key words: electrode resistance, solid electrolytes, oxygen transfer mechanism, complex impedance.

Downloaded 22 Jun 2009 to 130.89.112.86. Redistribution subject to ECS license or copyright; see http://www.ecsdl.org/terms_use.jsp